Supporting Information for "Propagation Effects of Slanted Narrow Bipolar Events: A Rebounding-Wave Model Study"

Dongshuai Li[1,2], Alejandro Luque[2], Farhad Rachidi[3], Marcos Rubinstein[4],

Torsten Neubert[1], Yanan Zhu[5], Olivier Chanrion[1], Caitano da Silva[6],

Paul R. Krehbiel[6]

[1]National Space Institute, Technical University of Denmark (DTU Space), Kongens Lyngby, Denmark.

[2]Instituto de Astrofísica de Andalucía (IAA), CSIC, Granada, Spain.

[3]Electromagnetic Compatibility Laboratory, Swiss Federal Institute of Technology (EPFL), Lausanne, Switzerland.

[4]University of Applied Sciences and Arts Western Switzerland, Yverdon-les-Bains, Switzerland.

[5]Earth Networks, Germantown, Maryland, USA.

[6]Langmuir Laboratory for Atmospheric Research, New Mexico Institute of Mining and Technology, Socorro, USA.

Contents of this file

1. Introduction

2. Text S1 to S2

3. Figure S1 to S5

4. Table S1

Introduction This supplement contains additional information in support of the data and methods presented in the main text. **Text S1** describe the details of the discontinuity term related to the current discontinuity. **Figure S1** shows the side and top snapshot of the FDTD simulation for the vertical electric fields of the slanted dipole with $\theta = 0°$, $30°$, $60°$ and $90°$. **Figure S2** illustrates the electrostatic, induction and radiation components for both vertical and slanted dipoles at different distances. **Text S2** and **Figure S3** describe the transformation geometry of the slanted channel of NBE3. **Figure S4** shows the current distribution along the channel for the vertical NBE1, the vertical NBE3, and the slanted NBE3 without and with the extra current I_{extra}. **Figure S5** shows the current distribution along the channel for the vertical NBE#174 and the vertical NBE#92 and the slanted NBE#92. **Table S1** details the inferred features of the fast breakdowns corresponding to the NBEs reported from Rison et al. (2016); Karunarathne et al. (2016).

Text S1: The discontinuity term related to the current discontinuity

The so-called discontinuity term (Thottappillil et al., 1998; Thottappillil & Rakov, 2001),"turn-on" term (M. A. Uman & McLain, 1970; M. A. Uman Martin A. & McLain, 1970) or F factor (Rubinstein & Uman, 1990; Thottappillil & Rakov, 2001, 2005; Shao et al., 2004, 2005) should be considered if there is a current discontinuity at the propagation wave front. Note that the discontinuity term is only applicable if there is a current discontinuity (Thottappillil et al., 1998; Thottappillil & Rakov, 2001). The discontinuity term and its image are given by

$$
dE_{zc}^{disc} = \frac{dL'}{4\pi\epsilon_0} \left(\begin{array}{c} \frac{(z_p - (L'\cos\theta + H_1))(x_p - L'\sin\theta\cos\phi)}{c^2 R^3(L')} \sin\theta\cos\phi \\ + \frac{(z_p - (L'\cos\theta + H_1))(y_p - L'\sin\theta\sin\phi)}{c^2 R^3(L')} \sin\theta\sin\phi \\ - \frac{(z_p - (L'\cos\theta + H_1))^2 - R^2(L')}{c^2 R^3(L')} \cos\theta \end{array} \right) I(L', t - R(L')/c - (H_2 - r)/v)\frac{dL'}{dt}, \quad (1)
$$

and its image,

$$
dE_{zm}^{disc} = -\frac{dL'}{4\pi\epsilon_0} \left(\begin{array}{c} \frac{(z_p + (L'\cos\theta + H_1))(x_p - L'\sin\theta\cos\phi)}{c^2 R_0^3(L')} \sin\theta\cos\phi \\ + \frac{(z_p + (L'\cos\theta + H_1))(y_p - L'\sin\theta\sin\phi)}{c^2 R_0^3(L')} \sin\theta\sin\phi \\ - \frac{(z_p + (L'\cos\theta + H_1))^2 - R_0^2(L')}{c^2 R_0^3(L')} \cos\theta \end{array} \right) I(L', t - R_0(L')/c - (H_2 - r)/v)\frac{dL'}{dt},
$$

$$(2)$$

where L' and $\frac{dL'}{dt}$ are, respectively, the retarded channel length and the speed of the current wave front as seen by the observer at P. v is the propagation velocity. $\frac{dL'}{dt}$ can be expressed as Rubinstein & Uman (1990); Thottappillil & Rakov (2001, 2005); Shao et al. (2004, 2005),

$$
\frac{dL'}{dt} = \frac{v}{1 - (v/c)\cos(\alpha(L'))} = vF(L'), \quad (3)
$$

where $\alpha(L')$ is the angle between the direction of propagation and the line connecting the retarded position of the wave front and the observation point at P. The F factor is

$$
F(L') = \frac{1}{1 - (v/c)\cos(\alpha(L'))}. \quad (4)
$$

Text S2: The transformation geometry of the slanted channel of NBE3

As shown in Figure S3(a), we assume the plane containing the NBE channel is perpendicular to the transfer vector $T = (x'_1, y'_1, 0)$ (see the red vector) with a distance ρ from the observation point P' is at the origin (0, 0, 0). The injection point $R'_1 = (x'_1, y'_1, z'_1)$ and end point $R'_2 = (x'_2, y'_2, z'_2)$ of the NBE channel are at radial distances of r_1 and r_2 away from the observer, respectively, with the elevation angle θ'_{el} ranging from 62° to 63.5° and azimuth angle ϕ'_{az} ranging from 338° to 340° (see Figure 9 in the Supplementary Material of Rison et al. (2016)). Assuming the NBE current propagates downward, the direction vectors for R'_1 and R'_2 can be written as

$$\vec{u_1} = (\sin\theta'_1 \cos\phi'_1, \ \sin\theta'_1 \sin\phi'_1, \ \cos\theta'_1),$$

$$\vec{u_2} = (\sin\theta'_2 \cos\phi'_2, \ \sin\theta'_2 \sin\phi'_2, \ \cos\theta'_2),$$

(5)

where the polar angle $\theta' = 90° - \theta'_{el}$ and azimuthal angle $\phi' = \phi'_{az}$. The injection point R'_1 and the end point R'_2 can be calculated as

$$R'_1 = r_1\vec{u_1},$$

$$R'_2 = r_2\vec{u_2},$$

(6)

where the radial distance $r = \rho/\cos(\theta'_{el})$, $\rho = 3.3\,\text{km}$ is the length of the transfer vector T corresponding to the plane distance between the source and the observer (Rison et al., 2016).

Once R'_1 and R'_2 have been obtained, we focus on the transformation from the geometry shown in Figure S3(a) (named as A') to the geometry given by Figure S3(b) (named as A). The relationship between two different geometries is then written

$$A' = T + A,$$

(7)

where the transfer vector $T = (x'_1, y'_1, 0)$ by moving the injection point R'_1 of the NBE channel back to the Z axis. Finally, based on geometry A in Figure S3(b), the new end point $R_2 = R'_2 - T = (x'_2 - x'_1, y'_2 - y'_1, 0)$ and the new observation point $P = P' - T = (-x'_1, -y'_1, 0)$. The new azimuthal angle of the source ϕ and the new azimuthal angle of the observer ϕ_p, defined

4

counterclockwise from the positive x-axis (North direction), can be calculated as:

$$\phi = 270° - \arctan\left(\frac{|x_2' - x_1'|}{|y_2' - y_1'|}\right) = 249°,$$

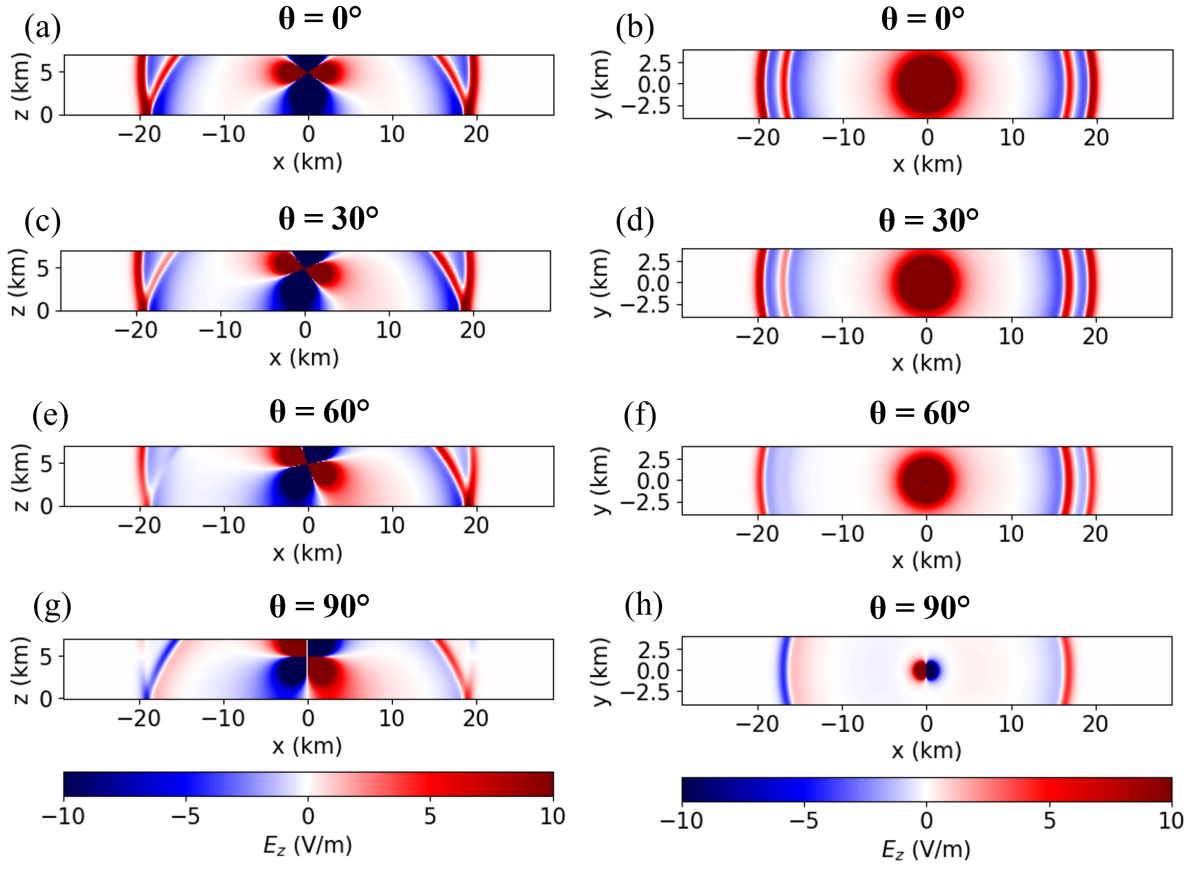$$\phi_p = 90 + \arctan\left(\frac{|-x_1'|}{|-y_1'|}\right) = 160°.$$

(8)

Table S1

Figure S1. Side (a,c,e,g) and top (b,d,f,h) view of a snapshot of the FDTD simulation for the vertical electric fields of the slanted dipole with the polar angle $\theta = 0°$ (vertical dipole), 30°, 60° and 90° (horizontal dipole).
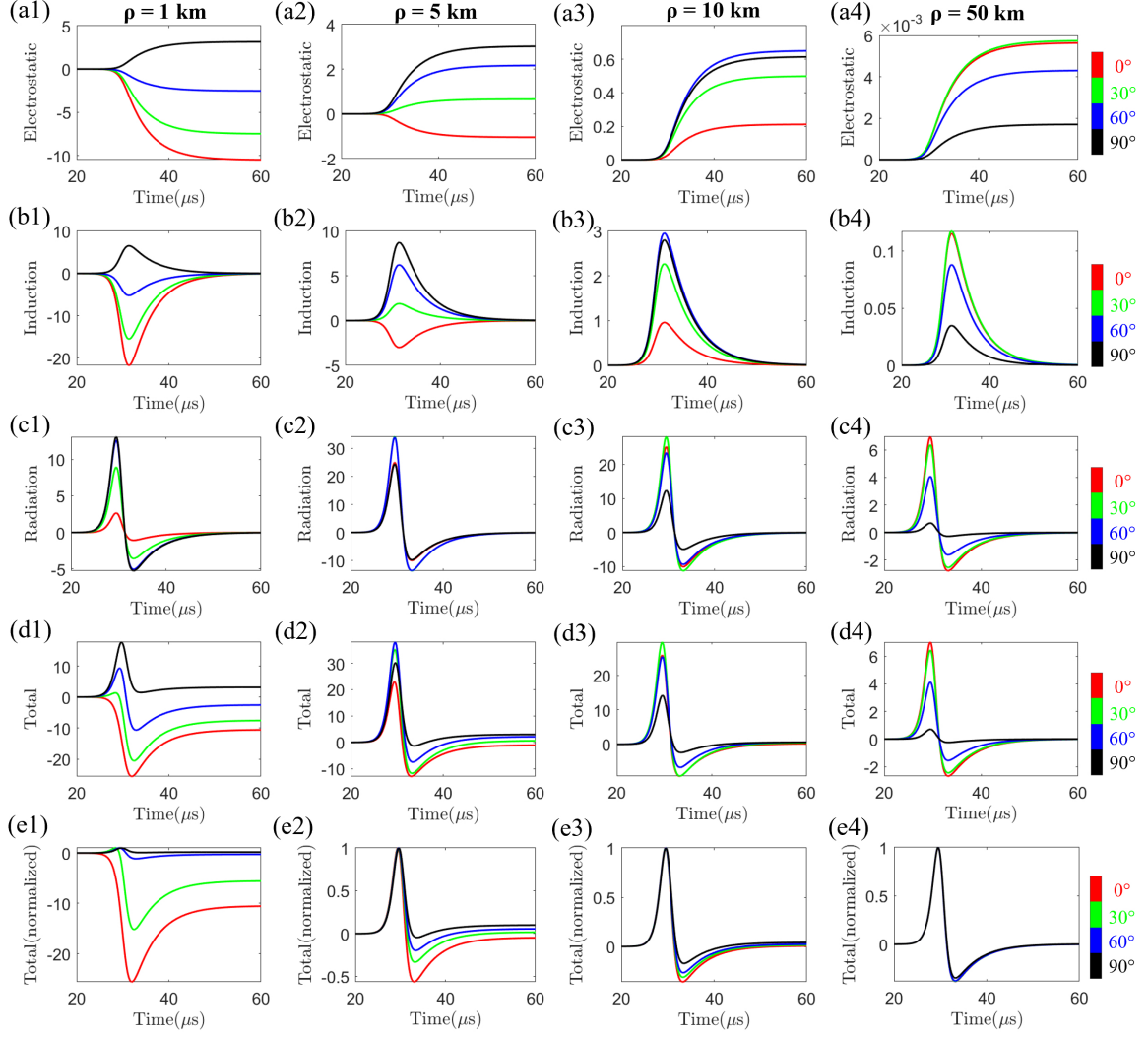
7

Figure S2. Electrostatic (a1-a4), Induction (b1-b4), and Radiation (c1-c4) components of the total electric fields (d1-d4) and the normalized total electric fields (e1-e4) for the slanted dipole with different θ angles with respect to Z axis and the azimuthal angle $\phi = 0°$ at a distance of 1 km, 5 km, 10 km and 50 km.
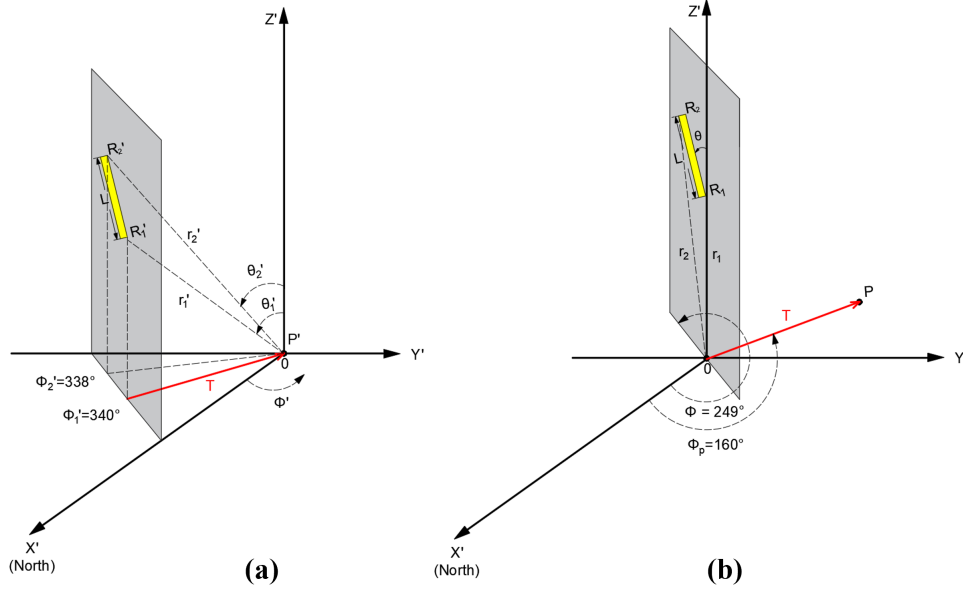
Figure S3. Schematic procedure to obtain the geometry of the slanted channel of NBE3. The transfer vector $T = (x'_1, y'_1, 0)$ from geometry A'(a) to A(b) is marked by the red arrow. (a) The geometry of the interferometer in Rison et al. (2016) (defined as A') with the observation point P' at the origin and the injection point R'_1 and the end point R'_2 of the NBE channel located at a plane that is perpendicular to the transfer vector T with a distance ρ. The azimuth angles for the channel ends range from $\phi'_2 = 338°$ to $\phi'_1 = 340°$ and (b) the geometry adopted in our study (defined as A) with the injection point R_1 of the NBE channel located on the Z axis and the observation point P located at T with a distance ρ and an azimuth angle $\phi_p = 160°$.

Figure S4. The downward, upward and total current distribution based on the rebounding MTLE model for the vertical NBE1(a1,b1,c1) and the vertical NBE3(a2,b2,c2), the slanted NBE3 without the extra current I_{extra}(a3,b3,c3) and the slanted NBE3 with the extra current I_{extra} (a4,b4,c4). The INTF data corresponding to the source time are marked by the pink dots.
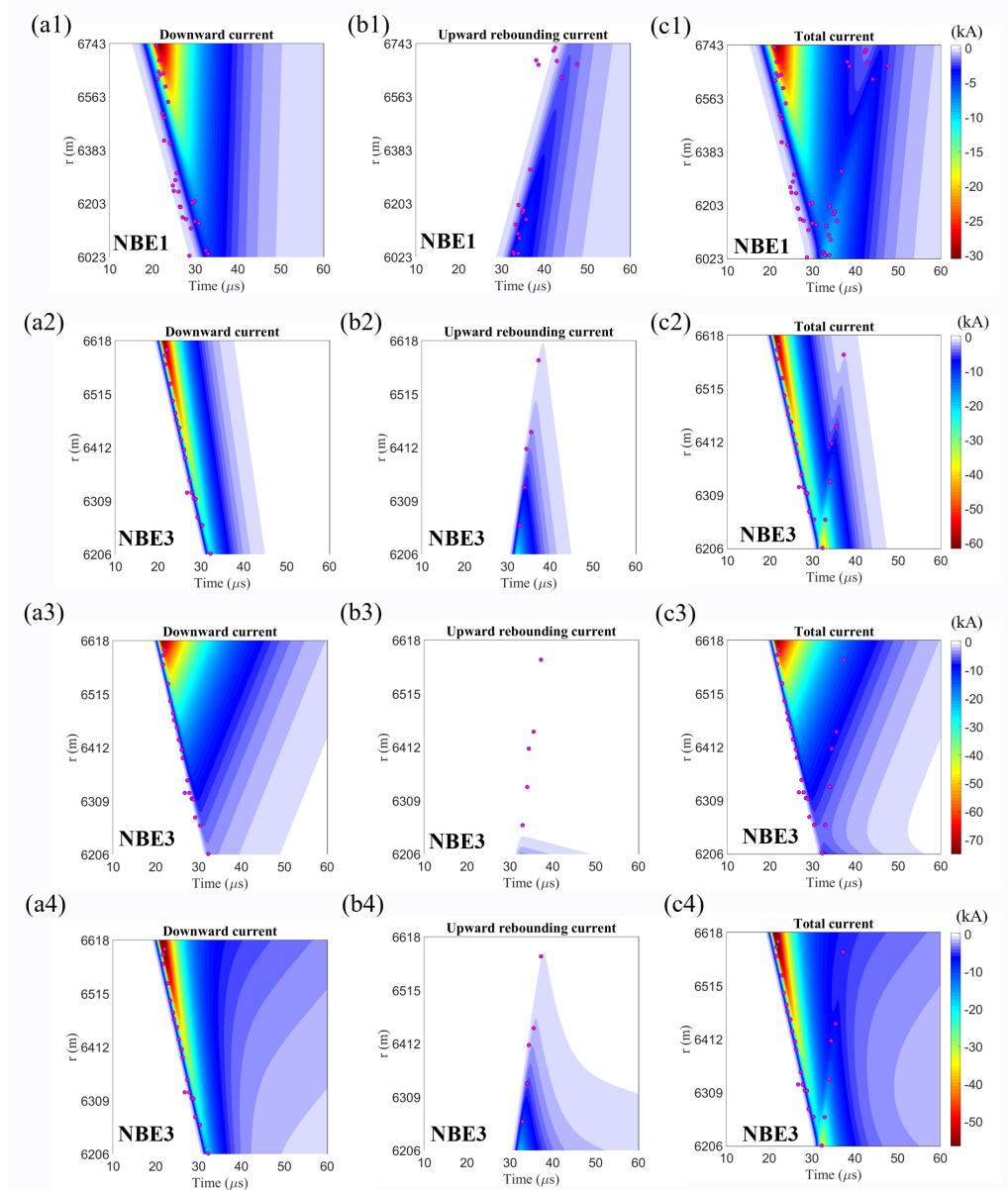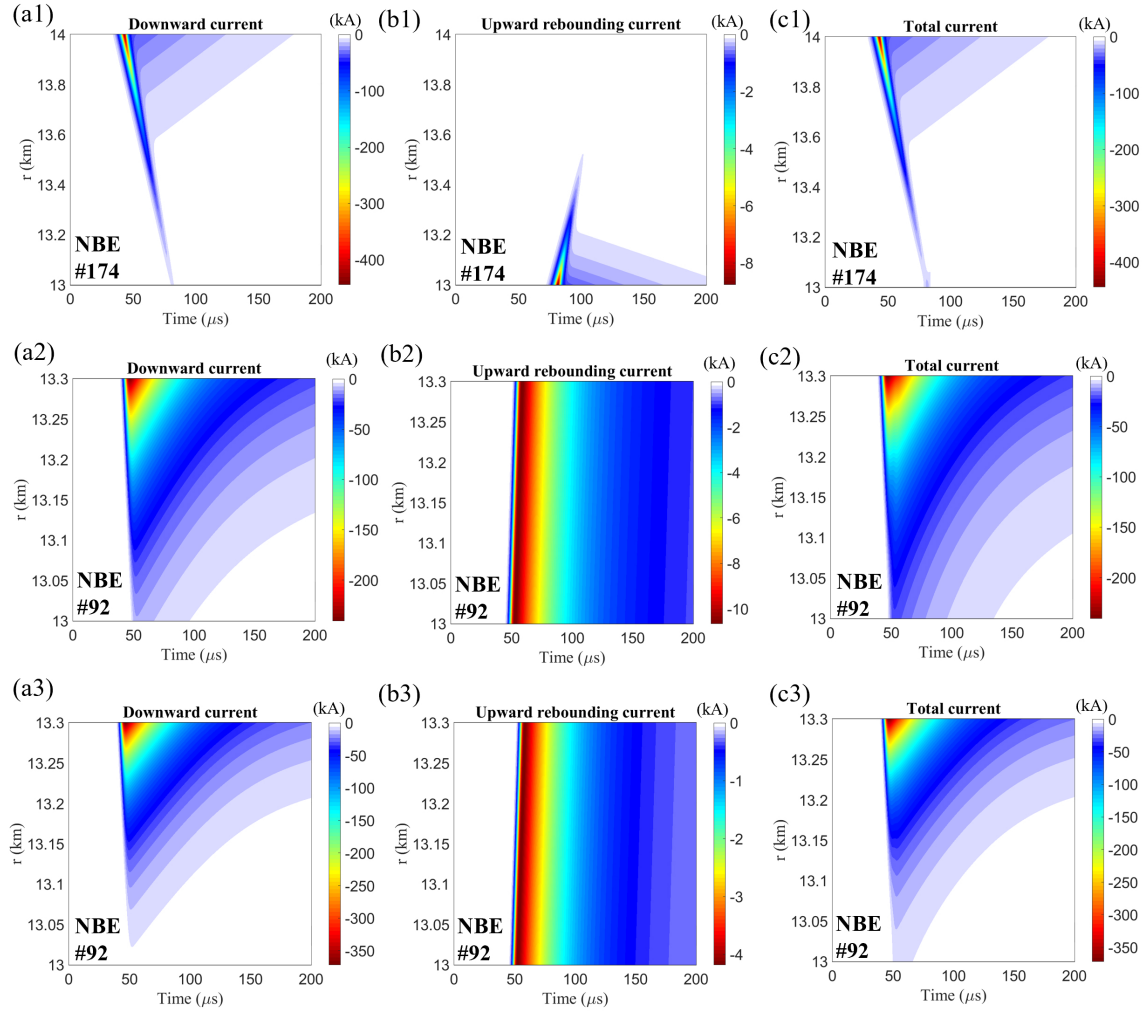
Figure S5. The downward, upward and total current distribution based on the rebounding MTLE model for the vertical NBE#174(a1,b1,c1) and the vertical NBE#92(a2,b2,c2) and the slanted NBE#92(a3,b3,c3) in Karunarathne et al. (2016).

Table S1. The inferred features of the fast breakdowns corresponding to the vertical NBE1, the vertical NBE3 , the slanted NBE3 without and with the extra current I_{extra}, the vertical NBE#174, the vertical NBE#92, and the slanted NBE#92.

ID	Inclination	Polar angle θ	Simulation-determined parameters								INTF-determined parameters				
			I_{peak}	τ_1	τ_2	I_{peak}^{extra}	τ_3	λ_d	λ_u	Q_{mom}	ρ	H_2	L	t_d^*	t_u^*
			(kA)	(μs)	(μs)	(kA)	(μs)	(m)	(m)	(C·m)	(km)	(km)	(m)	(μs)	(μs)
NBE1	Vertical	0°	-30.5	0.8	7.0	-	-	374.9	857.6	-215	5.5	6.7	720	12	13
NBE3	Vertical	0°	-61.7	0.3	3.4	-	-	378.7	113.7	-116	3.3	6.6	412	11	6
	Slanted	15°	-75	0.3	10.4	-	-	136.6	22.1	-357	3.3	6.6	412	11	6
	Slanted	15°	-56.6	0.3	3.2	-7.4	39.7	305.4	98.3	-219	3.3	6.6	412	11	6

ID	Inclination	Polar angle θ	Simulation-determined parameters								Other parameters		
			I_{peak}	τ_1	τ_2	I_{peak}^{extra}	τ_3	λ_d	λ_u	Q_{mom}	H_2	$L^\dagger$	$v^\dagger$
			(kA)	(μs)	(μs)	(kA)	(μs)	(m)	(m)	(C·m)	(km)	(m)	(m/s)
NBE#174	Vertical	0°	-426.5	2.0	1.2	-34.9	78.1	257.3	125.8	-4775	13	1000	2.6×10^7
NBE#92	Vertical	0°	-200.6	1.0	31.4	-41.0	196.0	96.2	1×10^5	-4519	13.3	300	5×10^7
	Slanted	13°	-345.2	0.9	32.6	-28.9	410.1	66.8	1×10^5	-6958	13.3	300	5×10^7

[*] The downward and upward propagation time t_d and t_u are determined by fitting the INTF traces for both NBE1 and NBE3 in Rison et al. (2016).
[†] The channel length L and the propagation velocity v are obtained from Karunarathne et al. (2016); Rison et al. (2016).

References

Karunarathne, S., Marshall, T. C., Stolzenburg, M., & Karunarathna, N. (2016). Electrostatic field changes and durations of narrow bipolar events. *Journal of Geophysical Research: Atmospheres*, *121*(17), 10,161-10,174. doi: https://doi.org/10.1002/2016JD024789

Rison, W., Krehbiel, P. R., Stock, M. G., Edens, H. E., Shao, X.-M., Thomas, R. J., ... Zhang, Y. (2016). Observations of narrow bipolar events reveal how lightning is initiated in thunderstorms. *Nature communications*, *7*, 10721. doi: 10.1038/ncomms10721(2016)

Rubinstein, M., & Uman, M. A. (1990). On the radiation field turn-on term associated with traveling current discontinuities in lightning. *Journal of Geophysical Research: Atmospheres*, *95*(D4), 3711-3713. doi: 10.1029/JD095iD04p03711

Shao, X.-M., Fitzgerald, T. J., & Jacobson, A. R. (2005). Reply to comment by Rajeev Thottappillil and Vladimir A. Rakov on "Radio frequency radiation beam pattern of return strokes: A revisit to theoretical analysis". *Journal of Geophysical Research: Atmospheres*, *110*(D24). doi: 10.1029/ 2005JD005889

Shao, X.-M., Jacobson, A. R., & Fitzgerald, T. J. (2004). Radio frequency radiation beam pattern of lightning return strokes: A revisit to theoretical analysis. *Journal of Geophysical Research: Atmospheres*, *109*(D19). doi: 10.1029/2004JD004612

Thottappillil, R., & Rakov, V. (2001). On the computation of electric fields from a lightning discharge in time domain. In *2001 IEEE EMC international symposium on electromagnetic compatibility* (Vol. 2, pp. 1030–1035).

Thottappillil, R., & Rakov, V. A. (2005). Comment on "Radio frequency radiation beam pattern of lightning return strokes: A revisit to theoretical analysis" by Xuan-Min Shao, Abram R. Jacobson,

and T. Joseph Fitzgerald, journal = Journal of Geophysical Research: Atmospheres. , *110*(D24). doi: 10.1029/2004JD005729

Thottappillil, R., Uman, M. A., & Rakov, V. A. (1998). Treatment of retardation effects in calculating the radiated electromagnetic fields from the lightning discharge. *Journal of Geophysical Research: Atmospheres*, *103*(D8), 9003-9013. doi: 10.1029/97JD02941

Uman, M. A., & McLain, D. K. (1970). Radiation field and current of the lightning stepped leader. *Journal of Geophysical Research (1896-1977)*, *75*(6), 1058-1066. doi: 10.1029/JC075i006p01058

Uman, M. A., Martin A., & McLain, D. K. (1970). Lightning return stroke current from magnetic and radiation field measurements. *Journal of Geophysical Research (1896-1977)*, *75*(27), 5143-5147. doi: 10.1029/JC075i027p05143